frontiers in Chemistry

ORIGINAL RESEARCH
published: 19 September 2018
doi: 10.3389/fchem.2018.00424

The Impact of Cr^{3+} Doping on Temperature Sensitivity Modulation in Cr^{3+} Doped and Cr^{3+}, Nd^{3+} Co-doped $Y_3Al_5O_{12}$, $Y_3Al_2Ga_3O_{12}$, and $Y_3Ga_5O_{12}$ Nanothermometers

*Karolina Elzbieciak and Lukasz Marciniak**

Institute of Low Temperatures and Structure Research PAS, Wrocław, Poland

A new approach to enhance the sensitivity of transition metal ion based nanocrystalline luminescent thermometer is presented. It was shown that the increase of Cr^{3+} concentration in three types of garnet host namely $Y_3Al_5O_{12}$, $Y_3Ga_5O_{12}$, and $Y_3Al_2Ga_3O_{12}$ allows for significant enhancement of their performance in non-contact thermometry. This phenomenon is related to the weakening of the crystal field strength due to enlargement of average Cr^{3+}-O^{2-} distance at higher Cr^{3+} concentrations. By increasing Cr^{3+} concentration from 0.6 to 30%, the sensitivity increased by over one order of magnitude from $S = 0.2\%/^{\circ}C$ to $S = 2.2\%/^{\circ}C$ at 9°C in $Y_3Al_2Ga_3O_{12}$ nanocrystals. Moreover, it was found that due to the $Cr^{3+} \rightarrow Nd^{3+}$ energy transfer in the Cr^{3+}, Nd^{3+} co-doped system, the usable Cr^{3+} concentration, for which its emission can be detected, is limited to 10% while the sensitivity at −50°C was doubled (from 1.3%/°C for $Y_3Al_2Ga_3O_{12}$:10%Cr^{3+} to 2.2%/°C $Y_3Al_2Ga_3O_{12}$:10%Cr^{3+}, 1%Nd^{3+} nanocrystals).

Keywords: chromium, luminescence, luminescent thermometers, Nanocrystals (NCs), garnets

OPEN ACCESS

Edited by:
Luís António Dias Carlos, University of Aveiro, Portugal

Reviewed by:
Xiaoji Xie, Nanjing Tech University, China
Chun Xu, The University of Queensland, Australia

****Correspondence:***
Lukasz Marciniak
l.marciniak@intibs.pl

Specialty section:
This article was submitted to Nanoscience, a section of the journal Frontiers in Chemistry

Received: *21 June 2018*
Accepted: *28 August 2018*
Published: *19 September 2018*

Citation:
Elzbieciak K and Marciniak L (2018) The Impact of Cr^{3+} Doping on Temperature Sensitivity Modulation in Cr^{3+} Doped and Cr^{3+}, Nd^{3+} Co-doped $Y_3Al_5O_{12}$, $Y_3Al_2Ga_3O_{12}$, and $Y_3Ga_5O_{12}$ Nanothermometers. Front. Chem. 6:424. doi: 10.3389/fchem.2018.00424

INTRODUCTION

In response to the requirements imposed by technology, micro/nanoelectronics or photonics as well as by biomedical applications, new approaches to the luminescent nanothermometers (LNTs) have to be proposed to secure fast and accurate temperature sensing with submicrometer spatial resolution, and highly sensitive temperature readout (Brites et al., 2012; Jaque and Vetrone, 2012; Chen et al., 2016; del Rosal et al., 2016a,b; Dramićanin, 2016; Marciniak et al., 2016b; Suo et al., 2017; Wang et al., 2017; Gao et al., 2018; Liao et al., 2018; Liu et al., 2018; Malysa et al., 2018; Runowski et al., 2018; Zhong et al., 2018). One of the most promising one, relies on exploiting transition metal (TM) ions, whose highly temperature dependent emission is referred to emission of barely temperature dependent lanthanides ions (Marciniak et al., 2017a; Drabik et al., 2018; Elzbieciak et al., 2018; Kniec and Marciniak, 2018; Marciniak and Trejgis, 2018; Trejgis and Marciniak, 2018). Materials which could be applied as real time temperature sensors in biomedicine, must also accomplish some other important requirements like sufficient sensitivity to temperature changes, high stability, low cytotoxicity (Brites et al., 2012; Jaque and Vetrone, 2012; Benayas et al., 2015) and operation in spectral range of optical transparency windows of biological tissues (Anderson and Parrish, 1981; Jaque and Jacinto, 2016). Because the transition metal ions based luminescent nanothermometers meet abovementioned flagship demands, they

can be considered as distinctively attractive research area. However, in order to be applicable, the thorough understanding of the correlation between structure of the host material and the thermal quenching of luminescence has to be studied. In our previous work (Elzbieciak et al., 2018), we have shown that by appropriate adjustment of the stoichiometry of the host matrix, relative sensitivity of Cr^{3+} ions-based luminescent thermometer can be intentionally modulated. The presented tuning occurred as a result of modification of the metal-to-oxygen ionic distance, which modified the strength of the crystal field (CF) (Struve and Huber, 2000; Xu et al., 2017). Therefore, taking advantage from the fact that CF influences the position of $^4T_2$ parabola, the activation energy, responsible for determination of thermal stability of luminescence, can be deliberately reduced. Efficient thermal quenching of the luminescence intensity is beneficial for sensitive luminescent thermometry. As it was already presented (Marciniak and Bednarkiewicz, 2016; Marciniak et al., 2016a, 2017b; Azkargorta et al., 2017), significant changes of the CF strength may also result from rising the concentration of active or passive dopants. Recently, Deren et al. (2012) showed that the increase of the Cr^{3+} concentration in $Y_3Ga_5O_{12}$:Cr^{3+} causes the diminishment of $^2E \rightarrow {}^4A_2$ narrow emission band and enhancement of $^4T_2 \rightarrow {}^4A_2$ band's intensity. Lowering the CF strength by growing number of Cr^{3+} ions, which is related with the elongation of the M-O distance, should relevantly enhance the relative sensitivity to temperature changes of such Cr^{3+} based luminescent thermometer. These observations motivated us to verify this hypothesis through comprehensive investigations of the impact of Cr^{3+} concentration (0.01–50%) on the temperature sensing capability in $Y_3Al_5O_{12}$, $Y_3Al_2Ga_3O_{12}$ and $Y_3Ga_5O_{12}$ nanocrystals.

EXPERIMENTAL

Nanopowders of (0.1; 0.5; 2; 5; 10; 20; 50%) Cr^{3+} and (0.1; 0.5; 2; 5; 10; 20; 50%) Cr^{3+},1% Nd^{3+} doped $Y_3Al_5O_{12}$, $Y_3Ga_5O_{12}$ and (0.06; 0.3; 1.2; 3; 6; 9; 12; 30%) Cr^{3+}, (0.06; 0.3; 1.2; 3; 6; 9; 12; 30%) Cr^{3+}, 1%Nd^{3+} doped $Y_3Al_2Ga_3O_{12}$ garnets were synthesized by the modified Pechini method (Pechini, 1967). Whole synthesis procedure was analogous as described in our earlier work (Elzbieciak et al., 2018). In brief, in order to obtain metal nitrates, calculated amount of yttrium oxide and neodymium oxide were dissolved in deionized water with addition of ultrapure nitric acid. After triple recrystallization process, yttrium or yttrium and neodymium nitrates were mixed together with aluminum, gallium and chromium nitrates. Afterwards, aqueous solution of citric acid and PEG was added to the mixture, than it was stirred for 3 h. In order to form a resin the obtained solution was heated for 1 week at 90°C.

All the synthesized materials were annealed for 16 h at 850°C. The following starting materials were used for synthesis: yttrium oxide (Y_2O_3 with 99.995% purity from Stanford Materials Corporation), neodymium oxide (Nd_2O_3 with 99.998% purity from Stanford Materials Corporation), aluminum nitrate nonahydrate ($Al(NO_3)_3{\cdot}9H_2O$ Puratronic 99.999% purity from Alfa Aesar), gallium(III) nitrate nonahydrate ($Ga(NO_3)_3{\cdot}9H_2O$ Puratronic 99.999% purity from Alfa Aesar), chromium nitrate nonahydrate ($Cr(NO_3)_3{\cdot}9H_2O$, 99.99% purity from Alfa Aesar), citric acid ($C_6H_8O_7$ with 99.5+% purity from Alfa Aesar) and poly(ethylene glycol) (PEG $C_2H_6O_2$ BioUltra 200 from Sigma).

All of the obtained materials were examined by XRD (X-ray diffraction) measurements carried out on PANalitycal X'Pert diffractometer, equipped with an Anton Paar TCU 1000 N temperature control unit, using Ni-filtered Cu-K_α radiation ($V = 40$ kV, $I = 30$ mA). Transmission electron microscope (TEM) images were taken using FEI TECNAI G2 X-TWIN microscope equipped with EDS detector. Powders were dispersed in methanol solution in ultrasounds and applied for lacey type copper lattices. The studies were performed in conventional TEM microscope with 300 keV parallel beam electron energy. Images were digitally recorded using the Gatan Ultrascan 1000XP.

Excitation spectra were measured using FLS980 Fluorescence Spectrometer form Edinburgh Instruments. Temperature dependent emission spectra were measured using 450 nm excitation line from laser diode and recorded using a Silver-Nova Super Range TEC Spectrometer from Stellarnet of 1 nm spectral resolution. Temperature during the measurement was controlled using the THMS 600 heating stage from Linkam (0.1°C stability and 0.1°C set point resolution).

RESULTS AND DISCUSSION

The yttrium aluminum/gallium garnets, crystallize in cubic structure with Ia3-d space group. As it is known, structures of these materials ($A_3B_2C_3O_{12}$) provide three types of cation sites, namely dodecahedral Y^{3+} site and also octahedral (B) and tetrahedral (C) Al^{3+}/Ga^{3+} sites which, because of similarity in ionic radii and the same coordination number, could be occupied by lanthanide Ln^{3+} (A) and transition metal ions TM^{3+} (B, C), respectively. Representative XRD patterns of $Y_3Al_2Ga_3O_{12}$:Cr^{3+} nanocrystals with different chromium concentration are presented in **Figure 1a**. All the reflection peaks correspond to the reference patterns confirming phase purity of the synthesized materials even for high dopant concentration (see also Supporting Information, **Figures S1–S5**). It is worth noting that in case of YAG (**Figures S2, S3**) and YGG (**Figures S4, S5**) with doping above 20% of Cr^{3+} ions, additional peaks occur in the XRD pattern. The cell parameter, as it can be seen in **Figure 1b**, is strongly affected by the Cr^{3+} concentration. In the case of YAG:Cr^{3+}, parameter *a* increases from 11.99 Å for 0.1%Cr^{3+} to 12.16 Å for 50%Cr^{3+}. On the other hand for YGG:Cr^{3+} an opposite tendency can be found –the *a* parameter decreases from 12.09 Å for 0.1%Cr^{3+} to 12.05 Å for 50%Cr^{3+}. This is due to differences in ionic radius between host ions Al^{3+} (67.5 pm) and Ga^{3+}(76 pm) ions being substituted by a larger dopant Cr^{3+} ions (75.5 pm). When atom with shorter ionic radius is substituted by atom with longer one, as in the case of $Y_3Al_5O_{12}$, the volume of the unit cell increases, due to the local expansion of the structure. This was also confirmed by the increase of the microstrains in the YAG structure (calculated using Rietveld refinement, **Figure S7**). On the other hand, in the case of

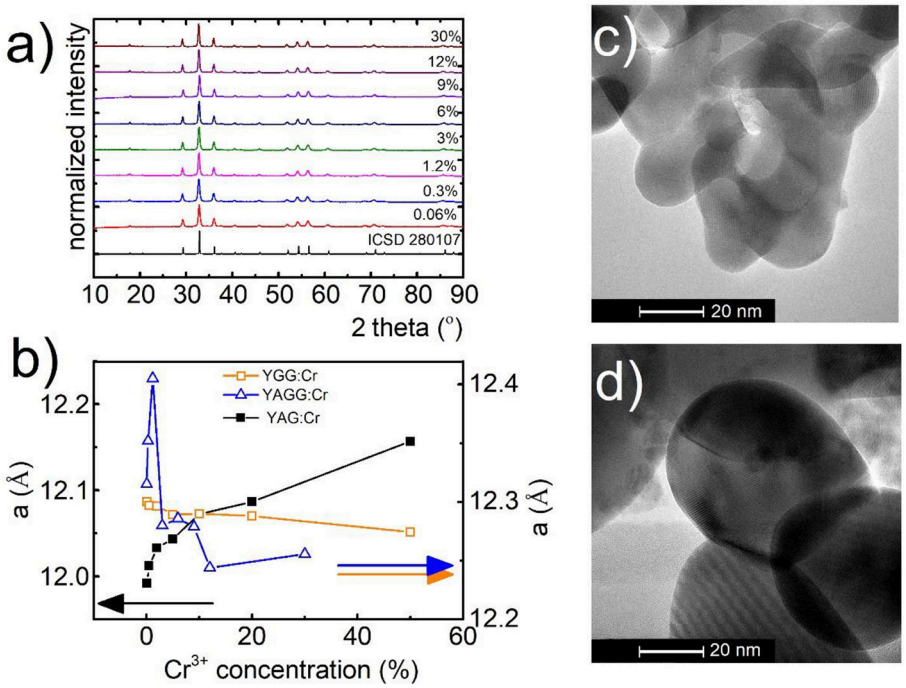

FIGURE 1 | Structural and morphological characterization of synthesized materials: XRD spectra for $Y_3Al_2Ga_3O_{12}$ **(a)** with different concentrations of Cr^{3+} ions, dependence of unit cell parameter **(a)** of YGG, YAG, and YAGG on Cr^{3+} concentration **(b)**; representative TEM images for $Y_3Al_2Ga_3O_{12}$:0.06%Cr^{3+},1%Nd^{3+} **(c)** and $Y_3Al_2Ga_3O_{12}$:30%Cr^{3+},1%Nd^{3+} **(d)** nanocrystals.

substitution of larger host ion with a smaller dopant ion, the parameter *a* and microstrains decrease likewise in the $Y_3Ga_5O_{12}$. The reduction of the cell parameter for increasing Cr^{3+} concentration observed in YAGG, is therefore a direct confirmation that Cr^{3+} ions substitute octahedral sites of Ga^{3+} ions. The average grain size of the nanocrystals, calculated using Rietveld refinement technique (around 60 nm), was in agreement with the nanoparticle size distribution determined from TEM images-70 ± 10 nm (**Figures 1c,d**, **Figure S6**). TEM images revealed good crystallization and some agglomeration of the obtained powders.

The simplified configurational coordinates diagram of Cr^{3+} is presented in **Figure 2A**. The luminescence of Cr^{3+} ions occurs through radiative depopulation of ^2E and/or $^4T_2$ states to the $^4A_2$ ground state. Due to the fact that strength of the crystal field determines the emission of Cr^{3+} ions, sharp emission line corresponding to the $^2E \rightarrow {}^4A_2$ transition and broadband emission corresponding to the $^4T_2 \rightarrow {}^4A_2$ transition can be observed in the emission spectra of Cr^{3+} ion in strong and weak crystal field, respectively. At higher temperatures, when the thermal energy is sufficient to reach the intersection point between the ^2E parabola and $^4T_2$ or $^4A_2$ parabolas, the process of nonradiative, multiphonon relaxation results in lowering of their emission intensity. Analysis of the emission spectra of $Y_3Al_2Ga_3O_{12}$:Cr^{3+} for different dopant concentration obtained upon 450 nm excitation, clearly indicates that at higher Cr^{3+} concentration the broad $^4T_2 \rightarrow {}^4A_2$ emission band localized at around 870 nm increase its intensity in respect to the $^2E \rightarrow {}^4A_2$ band at 692 nm (**Figure 2B**). Obviously, the total emission intensity decreases at higher dopant concentration due to the concentration quenching of luminescence. Nevertheless, it can be distinctly seen that $^4T_2 \rightarrow {}^4A_2$ dominates in the spectra for 30% of Cr^{3+} ions. Similar observation can be done in the emission spectra of $Y_3Al_5O_{12}$:Cr^{3+} and $Y_3Ga_5O_{12}$:Cr^{3+} nanocrystals presented in **Figures S8, S9**, respectively. However, in these cases similar trends can be observed for lower Cr^{3+} concentrations and to a lesser extent also in $Y_3Al_2Ga_3O_{12}$. Two main consequences of the lowering of $^4T_2$ state parabola can be found. First, at low dopant concentration the gradual reduction of its energy facilitates thermal depopulation of ^2E state–lowered ΔE_2 energy (the consequence of the intersection point between ^2E and $^4T_2$ parabolas). Secondly, at higher dopant concentration, when the energy $^4T_2$ state becomes lower than ^2E one, the broadband emission appears. The characteristic red-shift of the Cr^{3+} absorption bands localized around 400 nm and 575 nm, which can be attributed to the $^4A_2 \rightarrow {}^4T_1$ and $^4A_2 \rightarrow {}^4T_2$ electronic transitions, respectively, is a result of lowering of the CF strength (**Figures S12–S14**). In order to quantify the observed change of the crystal field strength in the examined nanocrystals, the Dq/B parameter was calculated for each of the samples as follows (Casalboni et al., 1994):

$$Dq = \frac{E\left({}^4A_2 \rightarrow {}^4T_2\right)}{10} \quad (1)$$

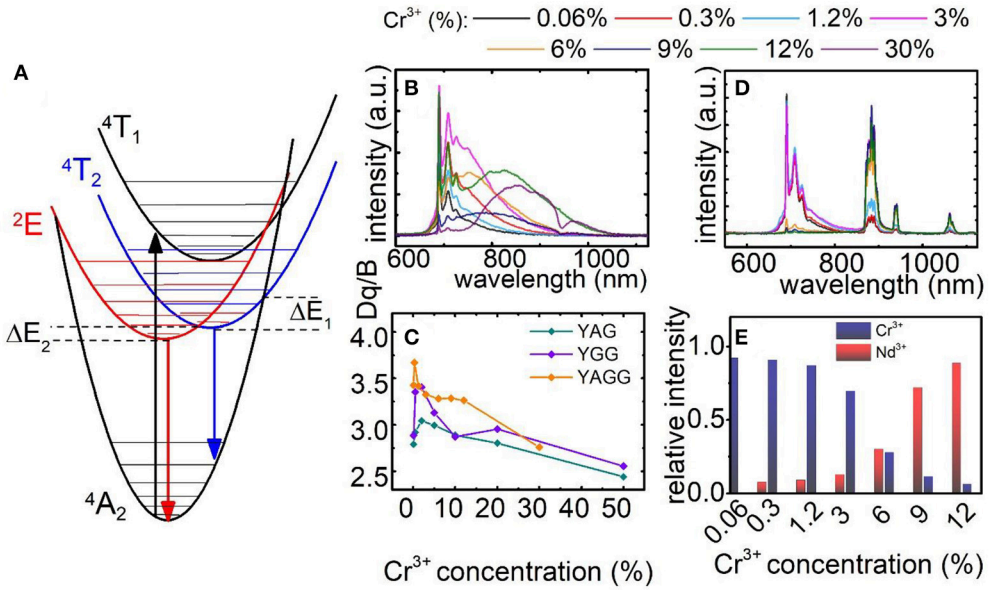

FIGURE 2 | Configurational coordinates diagram of Cr^{3+} ions **(A)**; comparison of normalized emission spectra for $Y_3Al_2Ga_3O_{12}$: xCr^{3+} **(B)** and for $Y_3Al_2Ga_3O_{12}$: xCr^{3+}, 1%Nd^{3+} nanocrystals **(D)**; dependence of Dq/B parameter **(C)** and Cr^{3+}/Nd^{3+} ratio at $T = -150°C$ **(E)** on Cr^{3+} concentration.

$$\frac{Dq}{B} = \frac{15\,(x-8)}{\left(x^2-10x\right)} \tag{2}$$

where x could be defined as (Casalboni et al., 1994):

$$x = \frac{E\left(^4A_2 \rightarrow {}^4T_1\right) - E\left(^4A_2 \rightarrow {}^4T_2\right)}{Dq} \tag{3}$$

As it can be observed in **Figure 2C** the Dq/B gradually decreases with Cr^{3+} concentration from 2.79 to 2.44 for $Y_3Al_5O_{12}$; from 2.88 to 2.55 for $Y_3Ga_5O_{12}$ and from 3.42 to 2.76 for $Y_3Al_2Ga_3O_{12}$ nanocrystals. In order to obtain self-referenced luminescent thermometer based of the Cr^{3+} emission intensity the examined nanocrystals with different Cr^{3+} concentration were co-doped with 1% Nd^{3+} ions. Emission intensity of Nd^{3+} is expected to be significantly less temperature dependent in respect to the chromium emission. Moreover, the Nd^{3+} ions emit in the first (band around 880 nm attributed to the $^4F_{3/2} \rightarrow {}^4I_{9/2}$ electronic transition) and the second (bands around 1064 nm and 1350 nm attributed to the $^4F_{3/2} \rightarrow {}^4I_{11/2}$ and $^4F_{3/2} \rightarrow {}^4I_{13/2}$ electronic transitions, respectively) optical window of the biological tissues making it well suited for biological applications.

Following excitation spectra, a 450 nm excitation line was chosen, which provides the condition of direct excitation of each individual optically active ion-Cr^{3+} ($^4A_2 \rightarrow {}^4T_1$) and independently Nd^{3+} ($^4I_{9/2} \rightarrow {}^2G_{5/2}$). As it was recently showed, this is an important condition to enhance the relative sensitivity of this kind of LTs (Marciniak et al., 2017a). In case of $Y_3Al_2Ga_3O_{12}$: Cr^{3+}, Nd^{3+} (**Figure 2D**) nanocrystals the presence of Nd^{3+} ion significantly quenched the Cr^{3+} emission intensity due to the $Cr^{3+} \rightarrow Nd^{3+}$ energy transfer. Therefore, the $^2E \rightarrow {}^4A_2$ emission band can be barely seen for $Y_3Al_2Ga_3O_{12}$: 30%Cr^{3+}, 1%Nd^{3+} while in the case of $Y_3Al_5O_{12}$ and $Y_3Ga_5O_{12}$ above 10% of Cr^{3+}, no chromium emission was detected (**Figures S10, S11**). Moreover, the presence of broad Cr^{3+} absorption bands in the excitation spectra when monitoring Nd^{3+} emission ($^4F_{3/2} \rightarrow {}^4I_{9/2}$ emission band), is an additional confirmation of the interionic energy transfer which takes place between dopants (**Figures S12–S14**). The change of contribution of the emission of particular optically active ions in the total emission intensity related with Cr^{3+} concentration is presented in **Figure 2E**. Initially, at low Cr^{3+} amount the $^2E \rightarrow {}^4A_2$ emission band dominates in the spectra. However, around 6% of Cr^{3+} its emission intensity equalize with Nd^{3+} amount. Above this value, the chromium emission intensity rapidly decreases. Therefore, this energy transfer strongly limits the usable Cr^{3+} concentration which can be applied for luminescent thermometry.

To understand the role of Cr^{3+} on the luminescence thermal quenching in the $Y_3Al_5O_{12}$ and $Y_3Ga_5O_{12}$ and $Y_3Al_2Ga_3O_{12}$ nanocrystals, their emission spectra were measured in a wide temperature range. The representative thermal evolution spectrum of $Y_3Al_2Ga_3O_{12}$:1.2%Cr^{3+} nanocrystals is presented in **Figure 3A**. It is clearly seen that sharp R-line of the $^2E \rightarrow {}^4A_2$ emission band is rapidly quenched at around 50°C in contrary to the $^4T_2 \rightarrow {}^4A_2$ emission. Therefore, due to this difference in the rates of thermal quenching of these particular emission bands, their luminescence intensity ratio was chosen as a temperature sensor LIR_1:

$$LIR_1 = \frac{Cr^{3+}(^4T_2 \rightarrow {}^4A_2)}{Cr^{3+}(^2E \rightarrow {}^4A_2)} = \frac{\int I(850-855)nm}{\int I(730-735)nm} \tag{4}$$

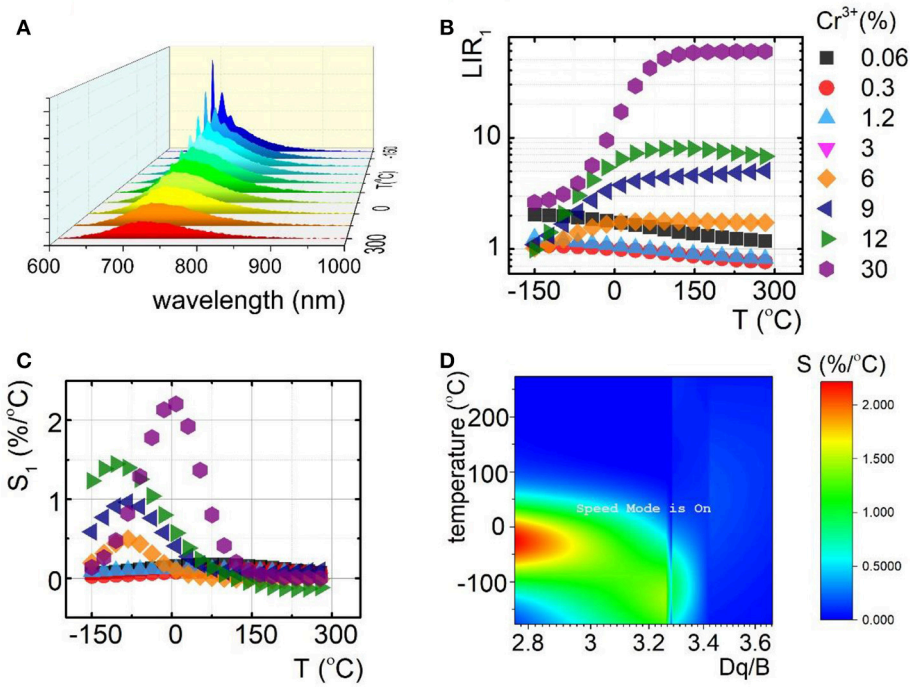

FIGURE 3 | Comparison of thermal evolution of emission spectra for $Y_3Al_2Ga_3O_{12}$:1.2%Cr^{3+} **(A)**; evolution of LIR_1 **(B)** with the corresponding relative sensitivities (S_1) **(C)** in the function of temperature; sensitivity map for different temperatures depending on Dq/B **(D)**.

At low Cr^{3+} concentration the LIR_1 decreases with temperature due to the fact that ^2E state population feeds the $^4T_2$ state at higher thermal energy. However, for higher Cr^{3+} (above 6%) different tendency can be found. Initially the LIR_1 increases up to temperatures around 100°C above which saturation of its value can be found. This effect occurs because $^4T_2 \rightarrow {}^4A_2$ band's intensity starts to play an important role in the total emission intensity. Due to the strong electron-phonon coupling, this emission band is expected to be efficiently reduced by the temperature. Therefore, its much higher rate of thermal quenching in respect to the $^2E \rightarrow {}^4A_2$ results in the enhancement of LIR_1 value. To quantitative describe the observed changes, relative sensitivity (S) of LIR_1-based luminescent thermometer was calculated according to the following formula:

$$S(T) = \frac{1}{LIR}\frac{\Delta LIR}{\Delta T}100\% \quad (5)$$

Independently from the Cr^{3+} concentration, the relative intensities reach maximal value at temperatures below 100°C. Above this value, low changes of LIR_1 are manifested as a minor value of S (**Figure 3C**). It is clearly seen that, according to our expectation, S significantly increases proportionally to Cr^{3+} content. The S_{max} at 9°C increases from 0.2%/°C for $Y_3Al_2Ga_3O_{12}$: 0.06%Cr^{3+} to 2.2%/°C for $Y_3Al_2Ga_3O_{12}$: 30%Cr^{3+} nanocrystals. Analogous tendency was found for the $Y_3Al_5O_{12}$:Cr^{3+} and $Y_3Ga_5O_{12}$:Cr^{3+} where for 10% Cr^{3+}, S_{max} equals to 2.7%/°C at −105°C and 2%/°C at −78°C respectively (**Figures S15, S16**). The observed enhancement of the rate of the thermal quenching is obviously caused by the lowering of the CF strength. The optically active ions in the heavily Cr^{3+}-doped nanocrystals are located in the lower CF sites (**Figure 3D**) which reduce the activation energy and facilitate luminescence thermal quenching. Therefore, the highest S were found for high Cr^{3+} concentration (low Dq/B values). However, above 130°C this correlation is suppressed due to the fact that above this temperature no $^2E \rightarrow {}^4A_2$ emission was observed. It is worth noting that the temperature range of high S overlaps with physiological temperature range (10–50°C) what indicates the importance of these LTs for biomedical applications.

Due to the fact that emission intensity of both $^2E \rightarrow {}^4A_2$ and $^4T_2 \rightarrow {}^4A_2$ bands decreases at higher temperatures, relative sensitivity of luminescent thermometer based on their intensity ratio is reduced. Therefore, Nd^{3+} co-dopant, whose emission intensity is expected to be less temperature dependent, were used as a luminescent reference. The luminescent properties of Nd^{3+}, Cr^{3+} co-doped nanocrystals were investigated in the analogous temperature range as in the case of singly Cr^{3+} doped counterparts. Representative thermal evolution of $Y_3Al_2Ga_3O_{12}$: 1.2%Cr^{3+}, 1%Nd^{3+} nanocrystals is presented in **Figure 4a**. According to the expectations the intensity of bands at 880 and 1,060 nm attributed to $^4F_{3/2} \rightarrow {}^4I_{9/2}$ and $^4F_{3/2} \rightarrow {}^4I_{11/2}$ electronic transition of Nd^{3+} ions, respectively, is almost independent on the temperature, while the $^2E \rightarrow {}^4A_2$ emission intensity is strongly thermally quenched. It is worth noting that at temperatures above 50°C, additional Nd^{3+} bands appears which

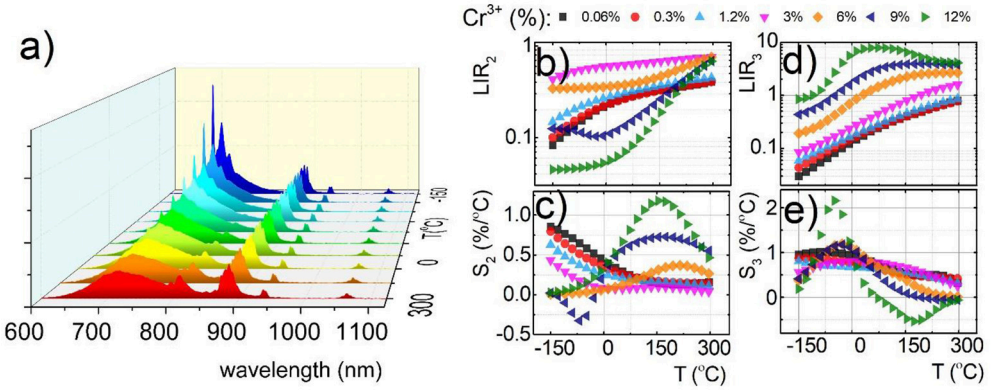

FIGURE 4 | Comparison of thermal evolution of emission spectra for $Y_3Al_2Ga_3O_{12}$:1.2%Cr^{3+}, 1%Nd^{3+} **(a)**; thermal evolution of LIR_2 **(b)**; and LIR_3 **(d)** and the corresponding relative sensitivities S_2 **(c)** and S_3 **(e)** for different Cr^{3+} concentration for $Y_3Al_2Ga_3O_{12}$:1.2%Cr^{3+}, 1%Nd^{3+} nanocrystals.

can be attributed to the $^4F_{5/2}$, $^4S_{3/2}\rightarrow{}^4I_{9/2}$ electronic transition. This band occurs at higher temperature due to the fact that population of $^4F_{5/2}$, $^4S_{3/2}$ states increases in respect to the $^4F_{3/2}$ with temperatures according to Boltzmann population. Taking advantage from these changes of the emission spectra with temperature, two types of luminescent thermometers based on the Nd^{3+}/Cr^{3+} luminescence intensity ratio have been defined as follows:

$$LIR_2 = \frac{Nd^{3+}(^4F_{3/2}\rightarrow{}^4I_{9/2})}{Cr^{3+}(^4T_2\rightarrow{}^4A_2)} = \frac{\int I(869-869.5)nm}{\int I(705-705.5)nm} \quad (6)$$

$$LIR_3 = \frac{Nd^{3+}(^4F_{5/2}\rightarrow{}^4I_{9/2})}{Cr^{3+}(^4T_2\rightarrow{}^4A_2)} = \frac{\int I(810-810.5)nm}{\int I(710-710.5)nm} \quad (7)$$

The thermal dependence of LIR_2 and LIR_3 for different concentration of Cr^{3+} ions are presented in **Figures 4b,d**, respectively. Obviously, due to the $Cr^{3+}\rightarrow Nd^{3+}$ energy transfer the usable concentration range of Cr^{3+} is strongly limited (to 12% Cr^{3+}). Independently from dopant concentration, both LIR_2 and LIR_3 increase at higher temperature due to the thermal quenching of $^4T_2\rightarrow{}^4A_2$ band of Cr^{3+} (**Figures 4b,d**). However, more rapid changes can be found for LIR_3 what is obviously related with the increase of the $^4F_{5/2}$, $^4S_{3/2}\rightarrow{}^4I_{9/2}$ emission band of Nd^{3+}. Both LIR_2 and LIR_3 are strongly modulated by the Cr^{3+} concentration. In agreement with the results obtained for singly Cr^{3+} doped systems, significant enhancement of LIR's thermal changes can be found. At heavily doped phosphors the activation energies of $^4T_2$ level is meaningfully diminished facilitating its nonradiative depopulation. Small activation energy is beneficial for enhancement of the relative sensitivity of luminescent thermometers. Therefore, these effects substantially affect the relative sensitivity of both S_2 and S_3 (**Figures 4c,e**). The highest S_2 at 150°C increases from 0.17%/°C for 0.06% of Cr^{3+} to 1.17%/°C for 12% of Cr^{3+} ions. On the other hand the S_3 at −48°C increases from 0.95%/°C for 0.06% of Cr^{3+} to 2.16%/°C for 12% of Cr^{3+} ions. Comparing these results with the **Figure 3**, evident profitable effect of the Nd^{3+} ions use as a luminescent reference can be found. The relative sensitivity for 0.06% Cr^{3+} increases from $S_1 = 0.14\%/°C$ to $S_2 = 0.17\%/°C$ and $S_3 = 0.95\%/°C$, while for 12% Cr^{3+} from $S_1 = 1.37\%/°C$ to $S_2 = 1.17\%/°C$ and $S_3 = 2.16\%/°C$. Analogous beneficial effect of high Cr^{3+} concentration can be found for $Y_3Ga_5O_{12}$:Cr^{3+}, Nd^{3+} as well as $Y_3Al_5O_{12}$:Cr^{3+}, Nd^{3+} (**Figures S10, S11**). It is also worth noting that the LIR_2 reveals high sensitivity at high temperature range (above 100°C) in contrast to LIR_3, which unveils good performance for non-contact temperature sensing at low temperatures (below 0°C). Therefore, by simultaneous employment of both of these thermometers the temperature range where high accuracy temperature readout can be achieved, is widened.

The highest recorded sensitivity ($S = 2.64\%/°C$) was found for YAG nanocrystals at −100°C for 10% of Cr^{3+} (**Figure S15B**) due to the fact of the lowest CF strength for this host material. Nevertheless, CF strength was tuned in the widest range for $Y_3Al_2Ga_3O_{12}$: Cr^{3+}, Nd^{3+} via the Cr^{3+} doping the enhancement of S_3 was the strongest in this case. The most important finding presented in this paper is that highly sensitive luminescent thermometers can be intentionally designed by the modification of the CF strength through elongation of Cr^{3+}-O^{2-} distance and enlargement of the Cr^{3+} concentration.

CONCLUSIONS

In this work, we proposed a new strategy to modulate the relative thermal sensitivity of Cr^{3+} doped nanophosphors. We considered three types of garnet matrices doped with different Cr^{3+} concentrations, with or without Nd^{3+} co-dopant. It was shown that the increase of the Cr^{3+} concentration causes elongation of the average Cr^{3+}-O^{2-} distance leading to the reduction of the crystal field strength in $Y_3Al_2Ga_3O_{12}$, $Y_3Ga_5O_{12}$ and $Y_3Al_5O_{12}$ nanocrystals. A gradual increase of the broad emission band attributed to the $^4T_2\rightarrow{}^4A_2$ spin allowed transition of Cr^{3+} is observed. Moreover, the reduction of the $^4T_2$ state energy facilitates thermal quenching of ^2E state. Therefore, the relative sensitivity of $^4T_2\rightarrow{}^4A_2$ to $^2E\rightarrow{}^4A_2$ emission intensity

increases from $S = 0.2\%/^{\circ}C$ for $0.06\%Cr^{3+}$ to $S = 2.2\%/^{\circ}C$ for $30\%Cr^{3+}$ at 9°C in $Y_3Al_2Ga_3O_{12}$ nanocrystals, from $S = 0.027\%/^{\circ}C$ for $0.5\%Cr^{3+}$ to $S = 2.7\%$ for $10\%Cr^{3+}$ at $-105^{\circ}C$ in $Y_3Al_5O_{12}$ nanocrystals, and from $S = 0.14\%/^{\circ}C$ for $0.5\%Cr^{3+}$ to $S = 2\%$ for $10\%Cr^{3+}$ at −78°C in $Y_3Ga_5O_{12}$ nanocrystals. In the case of Nd^{3+} co-doped nanocrystals, due to the $Cr^{3+} \rightarrow Nd^{3+}$ energy transfer, the usable concentration range of Cr^{3+} dopants is strongly reduced and no evidence of Cr^{3+} emission was found above 10% of Cr^{3+}. However, by taking advantage from this energy transfer and the fact that $^4F_{5/2}$, $^4S_{3/2} \rightarrow {}^4I_{9/2}$ emission intensity increases proportionally to the temperature according to the Boltzmann distribution, the relative sensitivities of luminescent thermometers defined as $^4F_{5/2}$, $^4S_{3/2} \rightarrow {}^4I_{9/2}$ to $^4T_2 \rightarrow {}^4A_2$ luminescence intensity ratio enhances from 1.3%/°C at −50°C without Nd^{3+} dopant to 2.2%/°C at −50°C for nanocrystals doped with Nd^{3+} ions $Y_3Al_2Ga_3O_{12}$: $10\%Cr^{3+}$, Nd^{3+}). The presented results confirm that the relative sensitivity of luminescent thermometers can be effectively modulated by the dopant concentration. Moreover, it was proved that the presence of Nd^{3+} dopant contributes to faster quenching of Cr^{3+} luminescence, what is favorable for highly sensitive non-contact luminescent thermometers. Our studies may be considered as a next step toward intentional designing of nanocrystalline luminescent thermometers with fully controllable thermooptical response.

AUTHOR CONTRIBUTIONS

All authors listed have made a substantial, direct and intellectual contribution to the work, and approved it for publication.

ACKNOWLEDGMENTS

The High sensitive thermal imaging for biomedical and microelectronic application project is carried out within the First Team programme of the Foundation for Polish Science co-financed by the European Union under the European Regional Development Fund.

SUPPLEMENTARY MATERIAL

The Supplementary Material for this article can be found online at: https://www.frontiersin.org/articles/10.3389/fchem.2018.00424/full#supplementary-material

REFERENCES

Anderson, R. R., and Parrish, J. A. (1981). The optics of human skin. *J. Invest. Dermatol.* 77, 13–19. doi: 10.1111/1523-1747.ep12479191

Azkargorta, J., Marciniak, L., Iparraguirre, I., Balda, R., Strek, W., Barredo-Zuriarrain, M., et al. (2017). Influence of grain size and Nd^{3+}concentration on the stimulated emission of LiLa1-xNdxP4O12crystal powders. *Opt. Mater. (Amst).* 63, 46–50. doi: 10.1016/j.optmat.2016.07.016

Benayas, A., del Rosal, B., Pérez-Delgado, A., Santacruz-Gómez, K., Jaque, D., Alonso Hirata, G., et al. (2015). Nd:YAG Near-Infrared Luminescent Nanothermometers. *Adv. Opt. Mater.* 3, 687–694. doi: 10.1002/adom.201400484

Brites, C. D., Lima, P. P., Silva, N. J., Millán, A., Amaral, V. S., Palacio, F., et al. (2012). Thermometry at the nanoscale. *Nanoscale.* 4:4799. doi: 10.1039/c2nr30663h

Casalboni, M., Luci, A., and Grassano, U. M. (1994). Optical spectroscopy of La3Ga5SiO14: Cr^{3+} crystals. *Phys. Rev. B.* 49, 3781–3790. doi: 10.1103/PhysRevB.49.3781

Chen, D., Liu, S., Zhou, Y., Wan, Z., Huang, P., and Ji, Z. (2016). Dual-activator luminescence of RE/TM:Y3Al5O12(RE = Eu^{3+}, Tb^{3+}, Dy^{3+}; TM = Mn^{4+}, Cr^{3+}) phosphors for self-referencing optical thermometry. *J. Mater. Chem. C.* 4, 9044–9051. doi: 10.1039/C6TC02934E

del Rosal, B., Carrasco, E., Ren, F., Benayas, A., Vetrone, F., Sanz-Rodríguez, F., et al. (2016a). Infrared-emitting QDs for thermal therapy with real-time subcutaneous temperature feedback. *Adv. Funct. Mater.* 26, 6060–6068. doi: 10.1002/adfm.201601953

del Rosal, B., Pérez-Delgado, A., Carrasco, E., Jovanović, D. J., Dramićanin, M. D., DraŽić, G., et al. (2016b). Neodymium-based stoichiometric ultrasmall nanoparticles for multifunctional deep-tissue photothermal therapy. *Adv. Opt. Mater.* 4, 782–789. doi: 10.1002/adom.201500726

Deren, P. J., Watras, A., Gagor, A., and Pazik, R. (2012). Weak crystal field in yttrium gallium garnet (YGG) submicrocrystals doped with Cr^{3+}. *Cryst. Growth Des.* 12, 4752–4757. doi: 10.1021/cg300435t

Drabik, J., Cichy, B., and Marciniak, L. (2018). A New Type of Nanocrystalline Luminescent Thermometers Based on Ti/Ti and Ti/Ln (Ln = Nd, Eu, Dy) Luminescence Intensity Ratio. *J. Phys. Chem. C* 122, 14928–14936. doi: 10.1021/acs.jpcc.8b02328

Dramićanin, M. D. (2016). Sensing temperature via downshifting emissions of lanthanide-doped metal oxides and salts. A review. *Methods Appl. Fluoresc.* 4:042001. doi: 10.1088/2050-6120/4/4/042001

Elzbieciak, K., Bednarkiewicz, A., and Marciniak, L. (2018). Temperature sensitivity modulation through crystal field engineering in Ga^{3+} co-doped Gd3Al5-xGaxO$_{12}$: $Cr3^{+}$, $Nd3^{+}$ nanothermometers. *Sens. Actuat. B Chem.* 269, 96–102. doi: 10.1016/j.snb.2018.04.157

Gao, Y., Cheng, Y., Huang, F., Lin, H., Xu, J., and Wang, Y. (2018). Sn^{2+}/Mn^{2+}codoped strontium phosphate ($Sr_2P_2O_7$) phosphor for high temperature optical thermometry. *J. Alloys Compd.* 735, 1546–1552. doi: 10.1016/j.jallcom.2017.11.243

Jaque, D., and Jacinto, C. (2016). Luminescent nanoprobes for thermal bio-sensing: Towards controlled photo-thermal therapies. *J. Lumin.* 169, 394–399. doi: 10.1016/j.jlumin.2015.03.037

Jaque, D., and Vetrone, F. (2012). Luminescence nanothermometry. *Nanoscale.* 4:4301. doi: 10.1039/c2nr30764b

Kniec, K., and Marciniak, L. (2018). The influence of grain size and vanadium concentration on the spectroscopic properties of YAG:V^{3+},$V^{5+}$and YAG: V, Ln3+(Ln^{3+} = Eu^{3+}, Dy^{3+}, Nd^{3+}) nanocrystalline luminescent thermometers. *Sens. Actuat. B Chem.* 264 382–390. doi: 10.1016/j.snb.2018.02.189

Liao, J., Wang, Q., Kong, L., Ming, Z., Wang, Y., Li, Y., et al. (2018). Effect of Yb3+concentration on tunable upconversion luminescence and optically temperature sensing behavior in Gd2TiO5:Yb^{3+}/Er^{3+}phosphors. *Opt. Mater. (Amst).* 75, 841–849. doi: 10.1016/j.optmat.2017.12.009

Liu, L., Sun, Z., Ma, C., Tao, R., Zhang, J., Li, H., et al. (2018). Highly sensitive and accurate optical thermometer through Er doped tellurite glasses. *Mater. Res. Bull.* 105, 306–311. doi: 10.1016/j.materresbull.2018.04.053

Malysa, B., Meijerink, A., and Jüstel, T. (2018). Temperature dependent Cr^{3+}photoluminescence in garnets of the type X3Sc2Ga3O12(X = Lu, Y, Gd, La). *J. Lumin.* 202, 523–531. doi: 10.1016/j.jlumin.2018.05.076

Marciniak, L., and Bednarkiewicz, A. (2016). The influence of dopant concentration on temperature dependent emission spectra in LiLa1–x–yEuxTbyP$_4$O$_{12}$ nanocrystals: toward rational design of highly-sensitive luminescent nanothermometers. *Phys. Chem. Chem. Phys.* 18, 15584–15592. doi: 10.1039/C6CP00898D

Marciniak, L., Bednarkiewicz, A., Drabik, J., Trejgis, K., and Strek, W. (2017a). Optimization of highly sensitive YAG:Cr^{3+}, Nd^{3+} nanocrystal-based

luminescent thermometer operating in an optical window of biological tissues. *Phys. Chem. Chem. Phys*. 19, 7343–7351. doi: 10.1039/C6CP07213E

Marciniak, Ł., Bednarkiewicz, A., Hreniak, D., and Strek, W. (2016a). The influence of Nd^{3+} concentration and alkali ions on the sensitivity of non-contact temperature measurements in $ALaP_4O_{12}$:Nd^{3+} (A = Li, K, Na, Rb) nanocrystalline luminescent thermometers. *J. Mater. Chem. C*. 4, 11284–11290. doi: 10.1039/C6TC03396B

Marciniak, L., Bednarkiewicz, A., Kowalska, D., and Strek, W. (2016b). A new generation of highly sensitive luminescent thermometers operating in the optical window of biological tissues. *J. Mater. Chem. C*. 4, 5559–5563. doi: 10.1039/C6TC01484D

Marciniak, L., Pilch, A., Arabasz, S., Jin, D., and Bednarkiewicz, A. (2017b). Heterogeneously Nd^{3+} doped single nanoparticles for NIR-induced heat conversion, luminescence, and thermometry. *Nanoscale*. 9, 8288–8297. doi: 10.1039/C7NR02630G

Marciniak, L., and Trejgis, K. (2018). Luminescence lifetime thermometry with Mn^{3+}-Mn^{4+} co-doped nanocrystals. *J. Mater. Chem. C* 6, 7092–7100. doi: 10.1039/C8TC01981A

Pechini, M. P. (1967). *US Pat*. No 3330697.

Runowski, M., Bartkowiak, A., Majewska, M., Martín, I. R., and Lis, S. (2018). Upconverting lanthanide doped fluoride NaLuF4:Yb^{3+}-Er^{3+}-Ho^{3+}- optical sensor for multi-range fluorescence intensity ratio (FIR) thermometry in visible and NIR regions. *J. Lumin*. 201, 104–109. doi: 10.1016/j.jlumin.2018.04.040

Struve, B., and Huber, G. (2000). The effect of the crystal field strength on the optical spectra of Cr^{3+} in gallium garnet laser crystals. *Appl. Phys. B*. 36, 195–201. doi: 10.1007/BF00704574

Suo, H., Hu, F., Zhao, X., Zhang, Z., Li, T., Duan, C., et al. (2017). All-in-one thermometer-heater up-converting platform YF_3 :Yb^{3+}, Tm^{3+} operating in the first biological window. *J. Mater. Chem*. C. 5, 1501–1507. doi: 10.1039/C6TC05449H

Trejgis, K., and Marciniak, L. (2018). The influence of manganese concentration on the sensitivity of bandshape and lifetime luminescent thermometers in $Y_3Al_5O_{12}$:Mn^{3+}, Mn^{4+}, Nd^{3+} nanocrystals. *Phys. Chem. Chem. Phys*. 20, 9574–9581. doi: 10.1039/C8CP00558C

Wang, C., Wadhwa, A., Cui, S., Ma, R., Qiao, X., Fan, X., et al. (2017). Dual mode temperature sensing through luminescence lifetimes of F- and O-coordinated Cr3+sites in fluorosilicate glass-ceramics. *RSC Adv*. 7, 52435–52441. doi: 10.1039/C7RA10864H

Xu, J., Ueda, J., and Tanabe, S. (2017). Toward tunable and bright deep-red persistent luminescence of Cr^{3+} in garnets. *J. Am. Ceram. Soc*. 100, 4033–4044. doi: 10.1111/jace.14942

Zhong, J., Chen, D., Peng, Y., Lu, Y., Chen, X., Li, X., et al. (2018). A review on nanostructured glass ceramics for promising application in optical thermometry. *J. Alloys Compd*. 763, 34–48. doi: 10.1016/j.jallcom.2018.05.348

Conflict of Interest Statement: The authors declare that the research was conducted in the absence of any commercial or financial relationships that could be construed as a potential conflict of interest.